Rock Mechanics and Rock Engineering (2019) 52:83–95
https://doi.org/10.1007/s00603-018-1568-0

ORIGINAL PAPER

# Examination of Mean Stress Calculation Approaches in Rock Mechanics

**Ke Gao**[1,2] · **John P. Harrison**[1]

Received: 9 February 2018 / Accepted: 3 August 2018 / Published online: 3 September 2018


## Abstract

The mean stress, as a fundamental statistical property of a group of stress data, is essential for stress variability characterisation. However, currently in rock mechanics, the mean stress is customarily and erroneously calculated by separately averaging the principal stress magnitudes and orientations. In order to draw the attention of our community to the appropriate approach for stress variability characterisation, here we compare the customary scalar/vector mean with that obtained by the mathematically rigorous tensorial approach—the Euclidean mean. Calculation of mean stress using both a small group of actual in situ stress measurement results and a large group of simulated stress data (obtained using the combined finite–discrete element method, FEMDEM) demonstrates that the two approaches yield different results. Further investigation of these results shows that the scalar/vector approach may yield non-unique and non-orthogonal mean principal stresses, and these may deviate significantly from those of the Euclidean mean. Our calculations and comparisons reveal that the scalar/vector approach is deficient because it processes the principal stress magnitudes and orientations separately as independent quantities and ignores the connection between them. Conversely, the tensorial approach appropriately averages the tensors that simultaneously carry not only the information of stress magnitudes and orientations, but also the inherent relations between them. Therefore, arbitrarily using scalar/vector mean stress of in situ stress measurements as input in further rock engineering analyses may yield significantly erroneous results. We advise that stress data should be statistically processed in a tensorial manner using tensors referred to a common Cartesian coordinate system.

**Keywords** Stress tensor · Rock mass · Mean stress · Euclidean mean · FEMDEM

### Abbreviations

| | |
|---|---|
| FEMDEM | Combined finite–discrete element method |

### List of symbols

| | |
|---|---|
| $E_p$ | Young's modulus of boundary plate |
| $E_r$ | Young's modulus of rock |
| $P_x$ | Boundary loading in $x$ direction |
| $P_y$ | Boundary loading in $y$ direction |
| $\mathbf{S}_i$ | $i$th stress tensor, $i = 1, 2, \ldots, n$ |
| $\bar{\mathbf{S}}_E$ | Euclidean mean stress tensor |
| $\varphi$ | Plunge of principal stress |
| $\bar{\varphi}$ | Mean of $\varphi$ |
| $\theta$ | Trend of principal stress |
| $\bar{\theta}$ | Mean of $\theta$ |
| $\sigma$ | Normal component of stress tensor |
| $\bar{\sigma}$ | Mean of $\sigma$ |
| $\sigma_1$ | Major principal stress |
| $\bar{\sigma}_1$ | Mean of $\sigma_1$ |
| $\sigma_2$ | Intermediate principal stress |
| $\bar{\sigma}_2$ | Mean of $\sigma_2$ |
| $\sigma_3$ | Minor principal stress |
| $\bar{\sigma}_3$ | Mean of $\sigma_3$ |
| $\tau$ | Shear component of stress tensor |
| $\bar{\tau}$ | Mean of $\tau$ |

✉ Ke Gao
k.gao@mail.utoronto.ca

[1] Department of Civil Engineering, University of Toronto, Toronto, Canada

[2] Present Address: Geophysics, Los Alamos National Laboratory, Los Alamos, NM, USA

## 1 Introduction

In situ stress is an important parameter for a wide range of endeavours in rock mechanics, including rock engineering design, hydraulic fracturing analysis, rock mass permeability and evaluation of earthquake potential (Amadei and Stephansson 1997; Latham et al. 2013; Matsumoto et al. 2015; Zang and Stephansson 2010; Zoback 2010). Because of the inherent complexity of fractured rock masses in terms

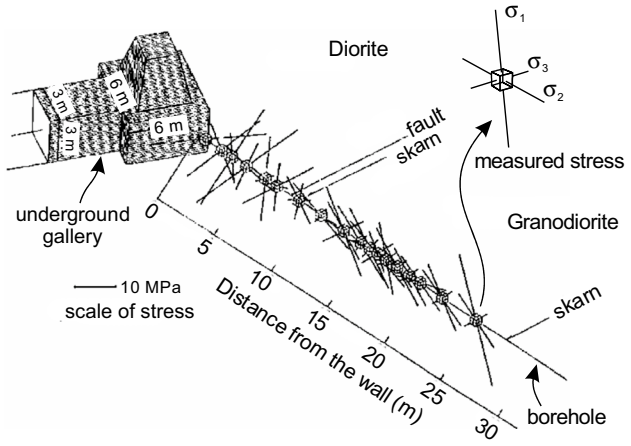


**Fig. 1** Stress change in terms of both principal stress magnitude and orientation observed near a fault. The pairs of orthogonal intersecting lines along the borehole represent the observed principal stresses at each location, with orientation being indicated directly and magnitude being proportional to line length (after Obara and Sugawara 2003)

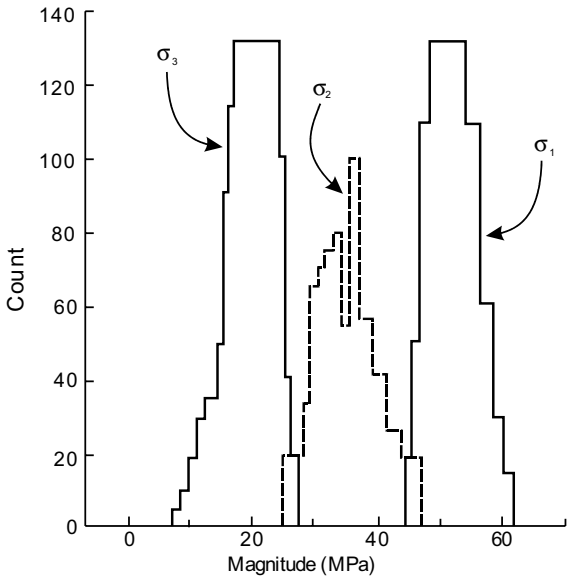


**(a)** Distribution of principal stress magnitudes

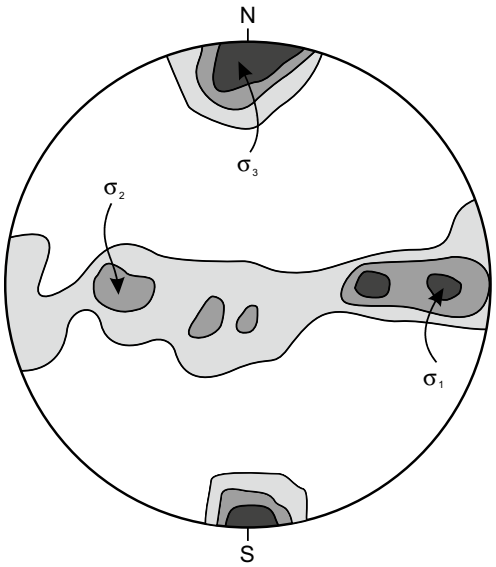


**(b)** Contouring of principal stress orientations

**Fig. 2** Scalar/vector analyses of stress examine principal stress magnitude and orientation separately using classical statistics and directional statistics, respectively (after Brady and Brown 2004)

of varying rock properties and the presence of discontinuities, stress in rock masses often displays significant variability (Day-Lewis 2008; Hyett 1990; Martin 1990; Matsumoto et al. 2015; Obara and Sugawara 2003). The in situ stresses measured along a borehole near an underground gallery shown in Fig. 1 exemplify the dramatic change in terms of both principal stress magnitude and orientation that may be observed in a small zone containing a fault (Obara and Sugawara 2003). Therefore, it is essential to develop rigorous statistical approaches for stress data processing and stress variability characterisation (Gao 2017; Gao and Harrison 2014, 2016a, b, 2018a, b; Lei and Gao 2018).

Mean stress is important not only because it is a fundamental statistical characteristic of a stress data group, but also because it is commonly used as an indicator of the overall stress state in a rock mass (Hakala et al. 2014; Han et al. 2016; Martin 2007; Martin et al. 2003; Martin and Simmons 1993; Siren et al. 2015). However, currently in rock mechanics, stress magnitude and orientation are commonly processed separately (Brown and Hoek 1978; Hakami 2011; Hast 1969; Herget 1988; Lisle 1989; Zhao et al. 2013). This effectively decomposes the stress tensor into scalar (principal stress magnitudes) and vector (principal stress orientations) components, and analyses them independently using classical statistics (Bulmer 1979) and directional statistics (Mardia 1972), respectively. One typical example is shown in Fig. 2, where histograms of principal stress magnitude and density contours of principal stress orientation are given. From these, statistics such as the mean principal stress magnitudes and orientations are calculated and used as input in further rock engineering analyses. However, this scalar/vector approach violates the tensorial nature of stress, and may either yield incorrect results or be difficult to interpret (Gao and Harrison 2014, 2015, 2017, 2018a, b; Hudson and Harrison 1997; Lei and Gao 2018). One manifest drawback of it is that orthogonality of the calculated mean principal stresses is not guaranteed.

Since stress is a second-order tensor, it should be processed based on stress tensors referred to a common Cartesian coordinate system. This has been advocated by several researchers (Dyke et al. 1987; Dzik et al. 1989; Hudson and Cooling 1988; Hyett et al. 1986; Jupe 1994; Koptev

et al. 2013; Martin et al. 1990; Martin and Simmons 1993; Walker et al. 1990). By considering the tensorial nature of stress, Gao and Harrison (2016b) give a rigorous derivation of how the mean stress can be calculated in a tensorial manner—the so-called Euclidean mean—based on the distance measure between stress tensors in Euclidean space. For example, when the $i$th stress tensor $\mathbf{S}_i$ is denoted by:

$$\mathbf{S}_i = \begin{bmatrix} \sigma_{x_i} & \tau_{xy_i} & \tau_{xz_i} \\ & \sigma_{y_i} & \tau_{yz_i} \\ \text{symmetric} & & \sigma_{z_i} \end{bmatrix}, \tag{1}$$

where $\sigma$ and $\tau$ are the normal and shear tensor components, respectively, then the Euclidean mean stress is given as the average of each tensor component, i.e.

$$\begin{aligned} \bar{\mathbf{S}}_{\mathrm{E}} = \frac{1}{n}\sum_{i=1}^{n}\mathbf{S}_i &= \begin{bmatrix} \bar{\sigma}_x & \bar{\tau}_{xy} & \bar{\tau}_{xz} \\ & \bar{\sigma}_y & \bar{\tau}_{yz} \\ \text{symmetric} & & \bar{\sigma}_z \end{bmatrix} \\ &= \frac{1}{n}\begin{bmatrix} \sum_{i=1}^{n}\sigma_{x_i} & \sum_{i=1}^{n}\tau_{xy_i} & \sum_{i=1}^{n}\tau_{xz_i} \\ & \sum_{i=1}^{n}\sigma_{y_i} & \sum_{i=1}^{n}\tau_{yz_i} \\ \text{symmetric} & & \sum_{i=1}^{n}\sigma_{z_i} \end{bmatrix}. \end{aligned} \tag{2}$$

Here, $\bar{\mathbf{S}}_{\mathrm{E}}$ denotes the Euclidean mean stress tensor, and $\bar{\sigma}$ and $\bar{\tau}$ denote the corresponding mean tensor components. This Euclidean mean essentially provides a theoretical support to the existing tensorial applications of calculating mean stress by averaging the corresponding stress tensor components (e.g., Dyke et al. 1987; Hudson and Cooling 1988; Koptev et al. 2013; Martin and Christiansson 1991a; Walker et al. 1990).

It seems that the incorrect scalar/vector mean stress calculation approach is still dominant in rock mechanics and rock engineering (e.g., Han et al. 2016; Siren et al. 2015; Valli et al. 2016; Veloso et al. 2015). In order to draw attention of our community to the correct approach for stress data processing, here, we demonstrate the reasons why the scalar/vector approach is inappropriate for stress variability characterisation and give a detailed investigation about how the scalar/vector mean may deviate from the tensorial Euclidean mean. Our goal is to unequivocally show that stress variability should be characterised in a tensorial manner based on stress tensors referred to a common Cartesian coordinate system.

In this paper, we first present an example calculation of the mean of two stress states to emphasise the deficiency of the scalar/vector approach and show the reason why stress data should be processed in a tensorial manner. Then, using actual in situ stress data (Martin 1990) and simulated stress data (Gao et al. 2017), we compare the scalar/vector and Euclidean means to demonstrate the inappropriateness of the scalar/vector approach and the rigorousness of the Euclidean mean. To facilitate the comparisons, we present the calculated mean stresses in terms of principal stress magnitude and orientation, unless otherwise mentioned.

## 2 Appropriateness of Scalar/Vector and Tensorial Approaches

As noted above, the scalar/vector approach of processing principal stress magnitude and orientation separately and independently may yield unreasonable results. Here, we represent the succinct and lucid example presented in Dyke et al. (1987) to emphasise this.

Let $\mathbf{S}_1$ and $\mathbf{S}_2$ be the two stress states

$$\mathbf{S}_1 = \begin{bmatrix} 18 & 0 \\ 0 & 10 \end{bmatrix} \quad \text{and} \quad \mathbf{S}_2 = \begin{bmatrix} 10 & 0 \\ 0 & 18 \end{bmatrix}, \tag{3}$$

referred to a common Cartesian coordinate system $x$–$y$. These stress states are also represented in Fig. 3a by ellipses whose semi-axes denote the magnitude and orientation of their principal values. $\mathbf{S}_1$ and $\mathbf{S}_2$ clearly possess identical principal stress magnitudes, but different principal stress orientations. Since the orientation of principal stress is bi-directional, the trend is ambiguous: the $\sigma_1$ trend for $\mathbf{S}_1$ (reckoned anticlockwise positive from the $x$-axis) may be considered as 000° or 180° with equal validity. Using these two values to calculate the mean orientation leads to either 045° (obtained using $\sigma_1$ trends of 000° and 090° for $\mathbf{S}_1$ and $\mathbf{S}_2$, respectively) or 135° (using 180° and 090°): directions that differ by 90°. These are shown as ellipses $A$ and $B$, respectively, in Fig. 3b. Clearly, this non-uniqueness is a significant deficiency of the scalar/vector calculation approach. In contrast, when the tensorial approach that averages the corresponding tensor components (i.e., Eq. 2) is applied, the unique mean symbolised by circle $C$ results (Fig. 3b).

The correctness of these two approaches can also be checked using the principle of superposition from solid mechanics: as Fig. 4 shows, superposition of stress states $\mathbf{S}_1$ and $\mathbf{S}_2$ results in

$$\mathbf{S}_1 + \mathbf{S}_2 = \begin{bmatrix} 18 & 0 \\ 0 & 10 \end{bmatrix} + \begin{bmatrix} 10 & 0 \\ 0 & 18 \end{bmatrix} = \begin{bmatrix} 28 & 0 \\ 0 & 28 \end{bmatrix}, \tag{4}$$

which is an isotropic stress state indicative of circle $C$ in Fig. 3b. Thus, the tensorial Euclidean mean,

$$\bar{\mathbf{S}}_{\mathrm{E}} = \frac{1}{2}(\mathbf{S}_1 + \mathbf{S}_2) = \begin{bmatrix} 14 & 0 \\ 0 & 14 \end{bmatrix}, \tag{5}$$

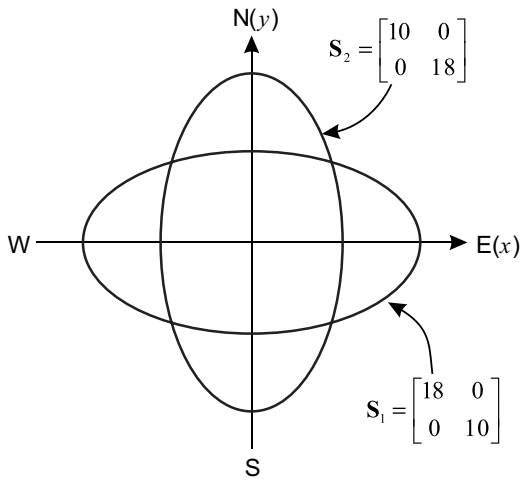


| Tensor | $\sigma_1$ (MPa) | $\sigma_2$ (MPa) | $\sigma_1$ trend |
|---|---|---|---|
| $\mathbf{S}_1$ | 18 | 10 | 090°/270° |
| $\mathbf{S}_2$ | 18 | 10 | 000°/180° |

**(a)** Principal stresses to be averaged

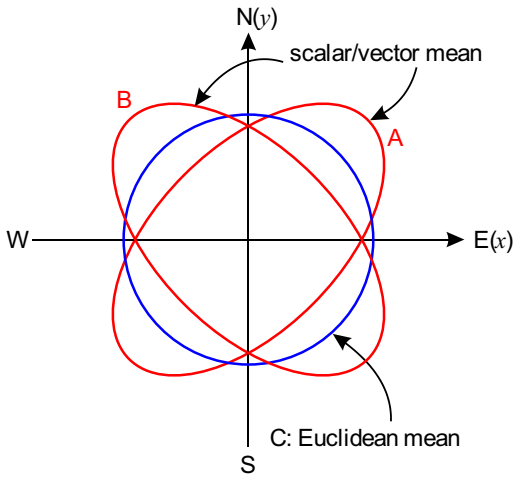


| Ellipse | $\sigma_1$ (MPa) | $\sigma_2$ (MPa) | $\sigma_1$ trend |
|---|---|---|---|
| A & B | 18 | 10 | 045°/225° & 135°/315° |
| C | 14 | 14 | -- |

**(b)** scalar/vector mean (A & B) and Euclidean mean (C)

**Fig. 3** Demonstration of stress tensor averaging using scalar/vector and tensorial approaches (after Dyke et al. 1987)

which is seen to be one-half the stress state obtained by superposition (Eq. 4), is clearly correct. In comparison, the scalar/vector approach, which averages the principal stress magnitudes and orientations separately, gives an anisotropic stress state, i.e., $\bar{\sigma}_1 = 18$ and $\bar{\sigma}_2 = 10$. This is evidently incorrect. The failure of the scalar/vector approach with this simple physical case is sufficient to demonstrate its incorrectness.

Another straightforward example is that of averaging the stress $\mathbf{S}_1$ (Eq. 3) and an isotropic stress state, say

$$\mathbf{S}_3 = \begin{bmatrix} 10 & 0 \\ 0 & 10 \end{bmatrix}. \tag{6}$$

Since the principal stress orientations of $\mathbf{S}_3$ could be any possible orthogonal combination, the scalar/vector mean of $\mathbf{S}_1$ and $\mathbf{S}_3$ is again non-unique. However, the Euclidean mean yields the unique result of

$$\bar{\mathbf{S}}_E = \frac{1}{2}(\mathbf{S}_1 + \mathbf{S}_3) = \begin{bmatrix} 14 & 0 \\ 0 & 10 \end{bmatrix}. \tag{7}$$

Although the above examples focus on calculating the mean stress, the fundamental reasoning applies also to the case of other statistical processing of stress data such as characterisation of probability density distribution (Gao and Harrison 2018a), generation of random stress tensors (Gao and Harrison 2017) and stress dispersion calculation (Gao and Harrison 2016a, 2018b). Thus, the conclusion to be drawn is that statistical analyses of stress data should use tensors referred to a common Cartesian coordinate system rather than separate processing of principal stress magnitude and orientation. To further support this assertion, in the sections below, both actual in situ and simulated stress data, representing small and large data groups respectively, are used to further examine the difference between the scalar/vector and Euclidean means.

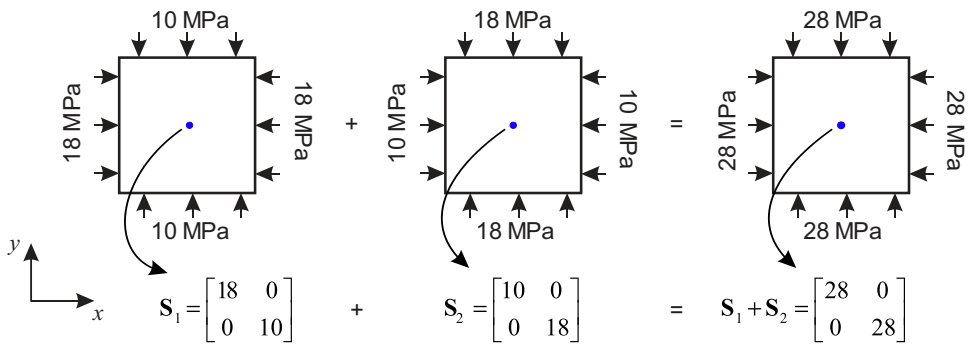


**Fig. 4** Physical interpretation of tensor addition as the superposition of stress states. Note that each matrix represents the stress tensor at the plate centre

## 3 Mean Stress Calculation of Actual In Situ Stress Data

As an example of actual stress data analysis, the mean stress is calculated using both scalar/vector and tensorial approaches for 19 in situ stress data. These data were obtained on the 300 level as part of the in situ stress measurement campaigns made at the Atomic Energy of Canada Limited's (AECL's) Underground Research Laboratory (URL) in southeastern Manitoba, Canada (Martin 1990). Geomechanics research was conducted at the AECL's URL during the period of about 1982–2004 to assess the feasibility of deep disposal of nuclear fuel waste in a plutonic rock mass (Chandler 2003; Martin 1990). These 19 stress data are part of the 99 in situ stress measurements presented by Martin (1990), which were made using a modified CSIR triaxial strain cell (Martin and Christiansson 1991b); they are used here to demonstrate the difference between scalar/vector and Euclidean means, rather than provide an interpretation of the stress conditions at the site. These data are presented in terms of principal stress magnitudes and orientations in Table 1.

For the scalar/vector mean, the mean principal stress magnitudes are calculated by averaging each principal stress separately, i.e.,

$$\bar{\sigma}_1 = \frac{1}{n}\sum_{i=1}^{n}\sigma_{1_i}, \quad \bar{\sigma}_2 = \frac{1}{n}\sum_{i=1}^{n}\sigma_{2_i}, \quad \bar{\sigma}_3 = \frac{1}{n}\sum_{i=1}^{n}\sigma_{3_i}, \tag{8}$$

and the principal stress orientations are calculated using directional statistics (Davis 1986, p. 333). For this, orientations are converted to unit vectors, namely

$$x_i = \cos(\varphi_i)\cdot\sin(\theta_i+\pi), \quad y_i = \cos(\varphi_i)\cdot\cos(\theta_i+\pi), \quad z_i = \sin(\varphi_i), \tag{9}$$

where the coordinate system is $x$ east, $y$ north and $z$ vertically upwards, and $\theta \in [0,\ 2\pi]$ (clockwise positive from North, looking downwards) and $\varphi \in [0,\ \pi/2]$ (positive from the horizontal plane to vertically upwards) denote the trend and plunge of principal stress, respectively (Fig. 5). The range ($[0,\ \pi/2]$) used here for plunge avoids ambiguous results caused by the bi-directional nature of principal stress orientation. The mean vector that denotes the mean orientation is:

$$\bar{x} = \left(\sum_{i=1}^{n} x_i\right)\Big/ L, \quad \bar{y} = \left(\sum_{i=1}^{n} y_i\right)\Big/ L, \quad \bar{z} = \left(\sum_{i=1}^{n} z_i\right)\Big/ L, \tag{10}$$

where

$$L = \sqrt{\left(\left(\sum_{i=1}^{n} x_i\right)^2 + \left(\sum_{i=1}^{n} y_i\right)^2 + \left(\sum_{i=1}^{n} z_i\right)^2\right)}. \tag{11}$$

The orientation of the scalar/vector mean principal stress is then

$$\begin{cases} \bar{\theta} = \begin{cases} \tan^{-1}(\bar{x}/\bar{y}) + \pi, & \text{if } \bar{y} > 0 \\ \mathrm{mod}\,(\tan^{-1}(\bar{x}/\bar{y}),\ 2\pi), & \text{if } \bar{y} \le 0\,. \end{cases} \\ \bar{\varphi} = \sin^{-1}(\bar{z}) \end{cases} \tag{12}$$

**Table 1** Nineteen actual in situ stress data obtained on the 300 level of the AECL's URL using the CSIR triaxial strain cell (data from Martin 1990)

| Depth (m) | $\sigma_1$ | | | $\sigma_2$ | | | $\sigma_3$ | | |
|---|---|---|---|---|---|---|---|---|---|
| | $\sigma_1$ (MPa) | Trend (°) | Plunge (°) | $\sigma_2$ (MPa) | Trend (°) | Plunge (°) | $\sigma_3$ (MPa) | Trend (°) | Plunge (°) |
| 302.53 | 34.98 | 313 | 08 | 21.56 | 049 | 38 | 18.98 | 213 | 51 |
| 302.54 | 37.79 | 316 | 16 | 22.12 | 225 | 04 | 17.16 | 121 | 73 |
| 302.59 | 36.79 | 346 | 02 | 22.72 | 079 | 61 | 19.39 | 255 | 29 |
| 302.64 | 40.12 | 314 | 10 | 23.04 | 220 | 18 | 21.7 | 070 | 69 |
| 302.67 | 27.08 | 332 | 52 | 22.98 | 064 | 01 | 20.09 | 155 | 38 |
| 302.68 | 39.44 | 316 | 13 | 22.73 | 216 | 38 | 18.19 | 050 | 61 |
| 302.69 | 39.65 | 263 | 05 | 20.21 | 353 | 01 | 16.37 | 093 | 85 |
| 302.71 | 51.82 | 267 | 07 | 30.89 | 358 | 12 | 20.63 | 147 | 76 |
| 302.72 | 49.71 | 274 | 09 | 27.6 | 182 | 11 | 21.56 | 043 | 76 |
| 302.73 | 47.42 | 263 | 07 | 26.28 | 355 | 10 | 22 | 141 | 78 |
| 302.78 | 45.46 | 281 | 04 | 24.54 | 011 | 04 | 22.98 | 151 | 85 |
| 302.80 | 42.14 | 082 | 03 | 26.02 | 173 | 30 | 16.14 | 347 | 60 |
| 302.83 | 42.35 | 272 | 11 | 29.75 | 181 | 01 | 24.67 | 084 | 79 |
| 302.97 | 52.47 | 005 | 09 | 36.34 | 096 | 05 | 27.59 | 212 | 80 |
| 302.98 | 58.05 | 010 | 12 | 36.23 | 105 | 22 | 19.94 | 253 | 65 |
| 302.99 | 42.21 | 011 | 11 | 30.16 | 101 | 02 | 21.24 | 198 | 79 |
| 303.01 | 37.26 | 200 | 00 | 24.59 | 290 | 15 | 19.58 | 109 | 75 |
| 303.02 | 27.69 | 050 | 22 | 23.14 | 308 | 26 | 19.29 | 175 | 55 |
| 303.02 | 36.23 | 001 | 06 | 26.26 | 093 | 19 | 22.26 | 254 | 70 |

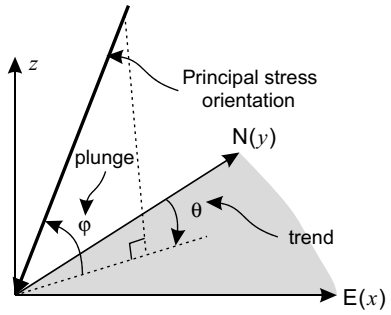


**Fig. 5** Demonstration of the coordinate system and principal stress trend and plunge for scalar/vector mean stress calculation for three-dimensional stress data

The Euclidean mean is calculated by first transforming all 19 in situ stress data into a common Cartesian coordinate system, say the *x*–*y*–*z* coordinate system used above, and then applying Eq. (2). The transformed tensors and their Euclidean mean are shown in Table 2. The eigenvalues and eigenvectors of the Euclidean mean represent the magnitudes and orientations of the principal mean stresses. These and the scalar/vector mean are shown in Table 3 and Fig. 6.

We observe that for these data, although the two approaches give similar orientation for $\bar{\sigma}_3$ (Fig. 6f), they lead to significantly different results for $\bar{\sigma}_1$ and $\bar{\sigma}_2$ (Fig. 6a–e). At first sight, it seems that the scalar/vector approach yields more reasonable results since the means of both the magnitudes and orientations are close to the centre of their respective data, whereas the mean principal stresses calculated by the Euclidean approach are located towards the periphery of the data (Fig. 6). However, this is an artefact of the scalar/vector approach as it separately averages the magnitude and orientation, and thus the calculated scalar/vector mean principal stress magnitudes and orientations are respectively located at the centre of each data cluster, as is shown in Fig. 6a–f.

**Table 2** In situ stress tensor components in *x*–*y*–*z* coordinate system and their Euclidean mean

| Depth (m) | Stress tensor components (MPa) | | | | | |
|---|---|---|---|---|---|---|
| | $\sigma_x$ | $\tau_{xy}$ | $\tau_{xz}$ | $\sigma_y$ | $\tau_{yz}$ | $\sigma_z$ |
| 302.53 | 28.20 | −7.05 | 0.69 | 27.00 | −2.37 | 20.31 |
| 302.54 | 28.93 | −7.09 | 3.93 | 29.46 | −3.64 | 18.67 |
| 302.59 | 21.14 | −3.92 | −1.20 | 35.78 | −0.96 | 21.98 |
| 302.64 | 31.21 | −8.29 | 2.47 | 31.33 | −2.06 | 22.32 |
| 302.67 | 23.05 | 0.02 | 1.69 | 22.66 | −2.94 | 24.44 |
| 302.68 | 25.45 | −9.89 | 6.58 | 30.38 | −2.25 | 24.53 |
| 302.69 | 39.19 | 2.31 | 2.04 | 20.49 | 0.14 | 16.55 |
| 302.71 | 51.30 | 1.09 | 3.84 | 30.51 | −1.89 | 21.53 |
| 302.72 | 48.88 | −1.82 | 4.39 | 27.47 | 0.93 | 22.52 |
| 302.73 | 46.59 | 2.97 | 3.27 | 26.56 | −0.30 | 22.55 |
| 302.78 | 44.52 | −3.97 | 1.81 | 25.31 | −0.53 | 23.15 |
| 302.80 | 41.70 | 2.55 | −1.98 | 23.87 | 4.07 | 18.73 |
| 302.83 | 41.66 | −0.81 | 3.34 | 29.79 | −0.24 | 25.32 |
| 302.97 | 36.29 | 1.07 | −1.34 | 51.79 | −3.75 | 28.32 |
| 302.98 | 33.99 | 2.71 | −6.90 | 56.26 | −6.14 | 23.97 |
| 302.99 | 30.58 | 2.20 | −1.31 | 40.99 | −3.78 | 22.04 |
| 303.01 | 25.79 | 4.20 | 1.15 | 35.72 | −0.51 | 19.92 |
| 303.02 | 25.62 | 2.10 | −0.97 | 23.22 | −2.77 | 21.28 |
| 303.02 | 25.83 | 0.09 | −1.26 | 36.09 | −1.37 | 22.84 |
| Euclidean mean | 34.21 | −1.13 | 1.07 | 31.83 | −1.60 | 22.16 |

**Table 3** Mean principal stress magnitudes and orientations of the 19 actual three-dimensional stress data calculated using both scalar/vector and tensorial approaches

| Mean | $\sigma_1$ | | | $\sigma_2$ | | | $\sigma_3$ | | |
|---|---|---|---|---|---|---|---|---|---|
| | $\sigma_1$ (MPa) | Trend (°) | Plunge (°) | $\sigma_2$ (MPa) | Trend (°) | Plunge (°) | $\sigma_3$ (MPa) | Trend (°) | Plunge (°) |
| Scalar/vector mean | 41.51 | 317 | 18 | 26.17 | 081 | 65 | 20.51 | 176 | 83 |
| Euclidean mean | 34.86 | 294 | 07 | 31.49 | 025 | 06 | 21.84 | 155 | 80 |

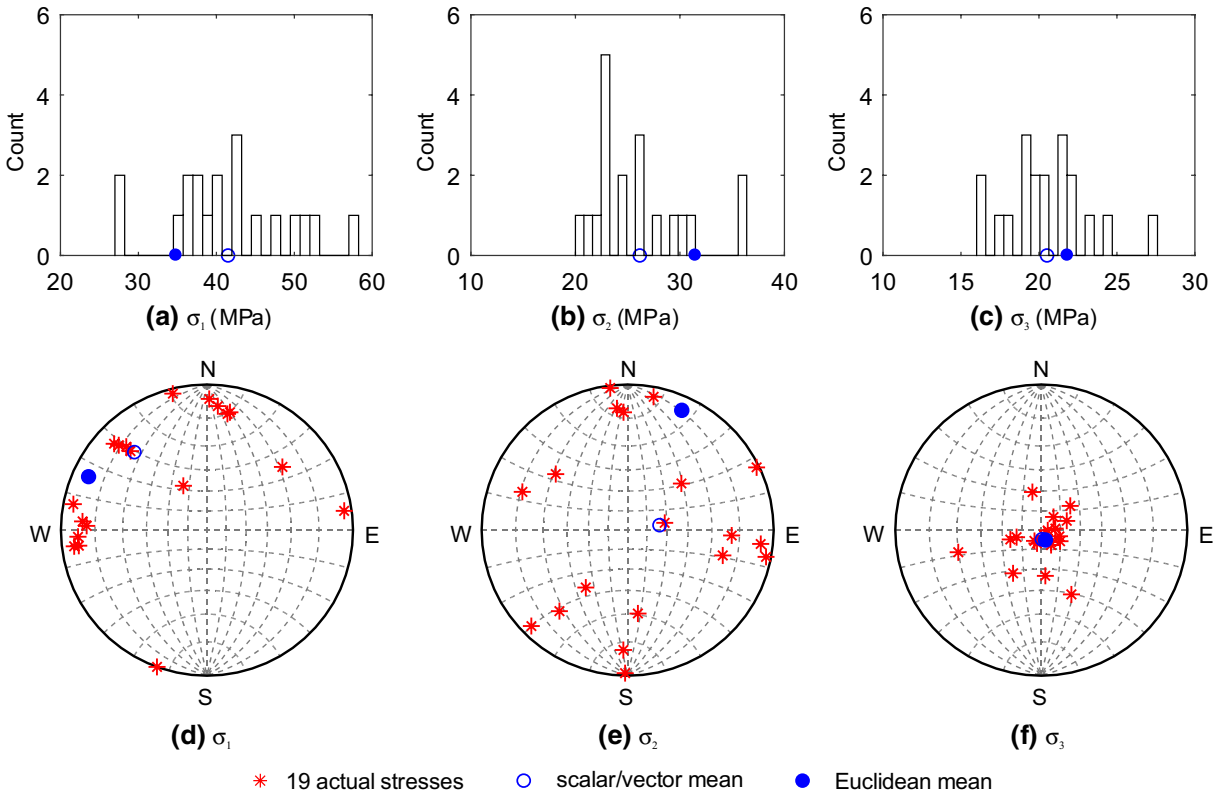


**Fig. 6** Histograms of the principal stress magnitude and hemispherical projections of principal stress orientation of the 19 three-dimensional actual in situ stress data, together with their scalar/vector and Euclidean means

Additionally, these results could lead one to observe that the Euclidean mean gives more extreme results than does the scalar/vector mean. This observation may be because currently in rock mechanics, stress data are commonly plotted in terms of principal stress magnitude and orientation using histograms and hemispherical projections, respectively (e.g., Fig. 2), and thus it is such results that are regarded as the norm. However, in this scalar/vector approach, the principal stress magnitudes are first sorted to distinguish the major, intermediate and minor principal stresses, and these are averaged separately. This is in stark contrast to the Euclidean mean, which averages complete stress tensors and thus considers the contributions of both stress magnitude and orientation simultaneously. The initial extraction and sorting of principal stress magnitudes means that the scalar/vector mean will generally yield larger $\sigma_1$ and smaller $\sigma_3$ than does the Euclidean mean, as can be seen from Fig. 6a, c, respectively. Since we have demonstrated in Sect. 2 that the Euclidean mean gives unique and physically correct results and thus should be used as the benchmark, we conclude that it is in fact the scalar/vector approach that gives more extreme results than does the Euclidean approach. Furthermore, and most importantly, with regard to orientation, a closer examination of the scalar/vector means reveals a lack of orthogonality of the principal mean stresses. Table 4 shows that the angle between $\bar{\sigma}_2$ and $\bar{\sigma}_3$ is about 26°, which is clearly incorrect by definition. In contrast, the Euclidean principal mean stresses are all guaranteed to be mutually orthogonal.

The fundamental reason for the scalar/vector approach yielding infeasible results is that it processes the principal stress magnitude and orientation separately, thereby implying that they are independent quantities and hence ignoring the inherent connection between principal stress magnitude and orientation. On the other hand, the tensorial approach obtains principal stress magnitudes and orientations as eigenvalues and eigenvectors, which are fundamental properties of the Euclidean mean.

**Table 4** Angles between the mean principal stress orientations of the 19 actual three-dimensional stress data calculated using both scalar/vector and tensorial approaches

| Mean principal stresses | $\sigma_1$ and $\sigma_2$ (°) | $\sigma_2$ and $\sigma_3$ (°) | $\sigma_3$ and $\sigma_1$ (°) |
|---|---|---|---|
| Scalar/vector mean | 87 | 26 | 78 |
| Euclidean mean | 90 | 90 | 90 |

Since rock engineering projects usually do not have the luxury of large numbers of in situ stress measurements for comprehensive statistical analysis, in the next section, numerical simulation (two-dimensional combined finite–discrete element method, FEMDEM) is used to generate a large group of stress data. These data are used to further examine the scalar/vector and Euclidean mean stress calculation approaches, and to check whether significant discrepancies between the two means still exist for larger stress data groups. We use two-dimensional simulated stress data to avoid the large computational cost of three-dimensional FEMDEM simulations. Additionally, it is straightforward to visualise two-dimensional stress states and this makes it easier to compare the difference between scalar/vector and Euclidean means. However, the analyses and reasoning in the current paper apply equally to both two- and three-dimensional stresses.

## 4 Mean Stress Calculation of Simulated Stress Data

The simulated stress data are obtained based on recent FEMDEM simulations (Gao et al. 2017) in which stress perturbation by discontinuities in a fractured rock mass are investigated. In this section, we first give an introduction of the model establishment and the FEMDEM code. Then the simulated stress data are used to compare the scalar/vector mean and Euclidean mean.

### 4.1 Model Establishment and FEMDEM Code

The $1.5 \times 1.5$-m rock mass model which contains two conjugate fracture sets striking roughly 140° and 100°, is extracted from an outcrop of the southern margin of the Bristol Channel Basin, UK (Belayneh et al. 2009), and used in current simulations. For stress-related simulations, the results have been shown to be influenced by the boundary conditions (Gao and Lei 2018). This earlier work examined the influence of the widely used stress boundary constraint and displacement boundary constraint on stress variability in a fractured rock mass. Stress boundary constraints (i.e., stress applied to the model boundary directly) prescribe stress values at the model boundary whilst allowing it to displace freely, whereas displacement boundary constraints (i.e., roller boundary conditions) prohibit the model boundary from moving in a normal direction, but leave the stresses at the boundary unconstrained. Importantly, neither of these widely used boundary conditions reflects the actual situation of a rock mass at depth. From the viewpoint of stiffness, these boundary conditions can be generalised as boundary plates with particular stiffness that confine the fractured rock mass. Through a series of tests that compared the influence of boundary constraint stiffness on overall stress variability, it was found that for the rock mass model used here, boundary plates with a thickness of 0.3 m and Young's modulus equal to that of the rock (i.e., $E_p = E_r$) are more appropriate than either the pure stress boundary constraints or displacement boundary constraints. The rock mass model together with the boundary condition used in the FEMDEM simulation is presented in Fig. 7.

The numerical tool—FEMDEM—used in this work, which was originally developed by Munjiza and colleagues, combines the advantages of both the finite element method (FEM) and discrete element method (DEM; Munjiza 2004; Xiang et al. 2009a, b). This tool has proven its efficacy and reliability as a computational tool to solve problems in a wide range of endeavours in rock mechanics such as stress analysis (Harrison et al. 2010; Latham et al. 2013; Lei and Gao 2018), permeability in a fractured rock mass (Latham et al. 2013) and rock fracture behaviour (Lei et al. 2014; Rougier et al. 2011). Importantly, FEMDEM allows one to explicitly realise the geometries of fracture patterns, and the embedded combined single and smeared crack model further permits the simulator to capture the emergence of new fracturing (Munjiza et al. 1999) thereby avoiding the potential unrealistic high stress concentrations at fracture tips. Together, these make it an ideal tool for stress heterogeneity modelling (Gao and Lei 2018).

FEMDEM for stress heterogeneity simulation has been validated previously (Lei and Gao 2018), with the results showing agreement between FEMDEM-simulated stress fields and analytical results for stress distribution around

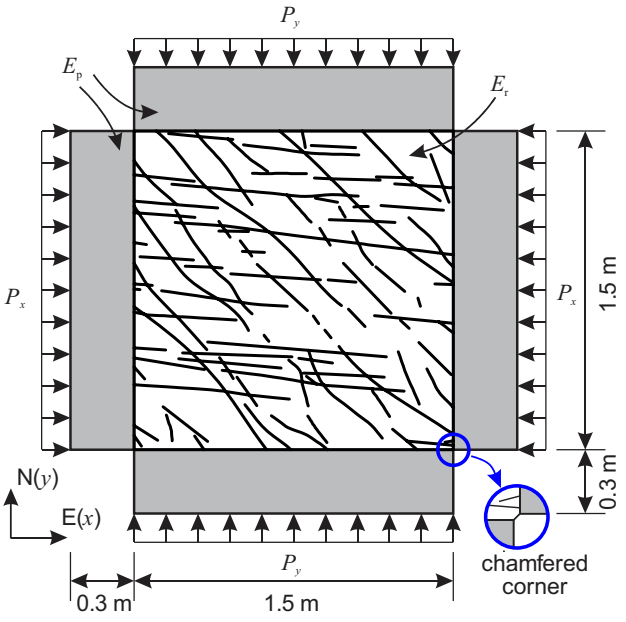


**Fig. 7** Schematic description of the model used for FEMDEM simulation (from Gao et al. 2017)

a single fracture under various conditions. FEMDEM is therefore able to generate realistic stress fields in a fractured rock mass and thus provide larger groups of stress data than those obtained from actual in situ stress measurements (e.g., Sect. 3). As a result, we are able to examine whether the differences between the scalar/vector mean and Euclidean mean are still significant for large groups of stress data.

In the current simulation, the rock mass comprises a total of 72,272 approximately uniformly meshed three-node constant strain triangular elements with an average element edge length of around 1 cm. Uniform compressive boundary loadings are increased gradually with increments of 1 and 2 Pa per time step until they reach the target values of $P_x = 5$ MPa and $P_y = 10$ MPa, respectively. When the model attains equilibrium, stress tensors from each element are extracted for further analysis. The distribution of major principal stress $\sigma_1$ of the simulation results is shown in Fig. 8.

## 4.2 Comparison Between Scalar/Vector Mean and Euclidean Mean

The scalar/vector mean of the simulated stresses are calculated by first decomposing the sampled stress tensors to obtain their principal stress magnitudes and orientations. The two mean principal stress magnitudes are calculated by averaging each of them, i.e., in a similar manner to Eq. (8).

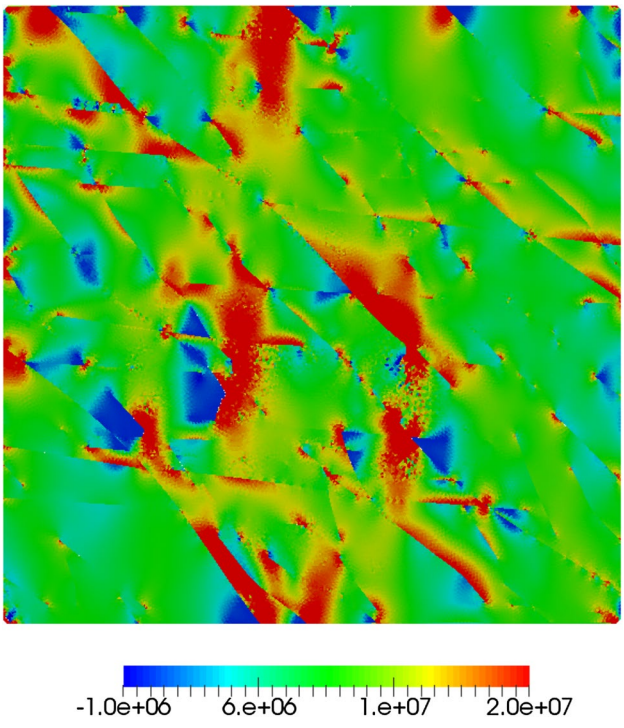


**Fig. 8** Distribution of major principal stress $\sigma_1$ (unit: Pa) under boundary loadings of $P_x = 5$ MPa and $P_y = 10$ MPa (after Gao et al. 2017)

Here, for simplicity and convenience, we use the trend of the major principal stress $\sigma_1$ to denote the orientation of principal stresses, as the trend of minor principal stress $\sigma_2$ can then be acquired accordingly. Since the trend of $\sigma_1$ is bi-directional, to avoid ambiguous results, only the trends of $\sigma_1$ located within the range of $[0,\ \pi]$ (clockwise positive from North) are considered (see Fig. 5). Using the coordinate system of $x$ east and $y$ north, the $x$ and $y$ coordinates of the unit vector representing the orientation of principal stress are:

$$\begin{cases} x = \sin(\theta) \\ y = \cos(\theta) \end{cases}, \tag{13}$$

where $\theta$ denotes the trend of major principal stress, $\sigma_1$. The scalar/vector mean principal stress orientation is calculated using directional statistics (Davis 1986, p. 316), i.e.,

$$\bar{\theta} = \mathrm{mod}\left( \tan^{-1}\left( \frac{\sum_{i=1}^{n} x_i}{\sum_{i=1}^{n} y_i} \right) + \pi, \pi \right). \tag{14}$$

The Euclidean mean is calculated using Eq. (2), with the eigenvalues and eigenvectors of the mean tensor giving the mean principal stress magnitudes and orientations, respectively. Both the scalar/vector and Euclidean means in terms of principal stresses are tabulated in Table 5, which, together with the probability density distributions of the sampled simulated stress data in terms of $\sigma_1$, $\sigma_2$ and $\theta$ are presented in Fig. 9. We observe that there is a distinct difference between the scalar/vector and Euclidean mean which is marked by the dashed lines in Fig. 9. The difference is further demonstrated by the Mohr's circle representation of the two means in Fig. 10. For the mean principal stress magnitudes, the scalar/vector mean gives larger $\sigma_1$ and smaller $\sigma_2$ than that of the Euclidean mean (Fig. 9a, b), which is similar to the mean calculation results shown previously using actual three-dimensional stress data. As for the mean principal stress orientation $\theta$, the scalar/vector mean deviates significantly from the Euclidean mean: here it is almost perpendicular to the Euclidean mean (Fig. 9c, d).

As mentioned earlier, the scalar/vector approach is deficient in that it processes the principal stress magnitudes and orientations as independent quantities and ignores the connection between them. In order to show that this is the case, correlation coefficients between $\sigma_1$ and $\sigma_2$ and $\theta$ of the

**Table 5** Scalar/vector mean and Euclidean mean of two-dimensional simulated stress data in terms of principal stresses

| Principal stresses | $\sigma_1$ (MPa) | $\sigma_2$ (MPa) | $\sigma_1$ trend (°) |
|---|---|---|---|
| Scalar/vector mean | 10.90 | 3.94 | 095 |
| Euclidean mean | 9.48 | 5.36 | 176 |

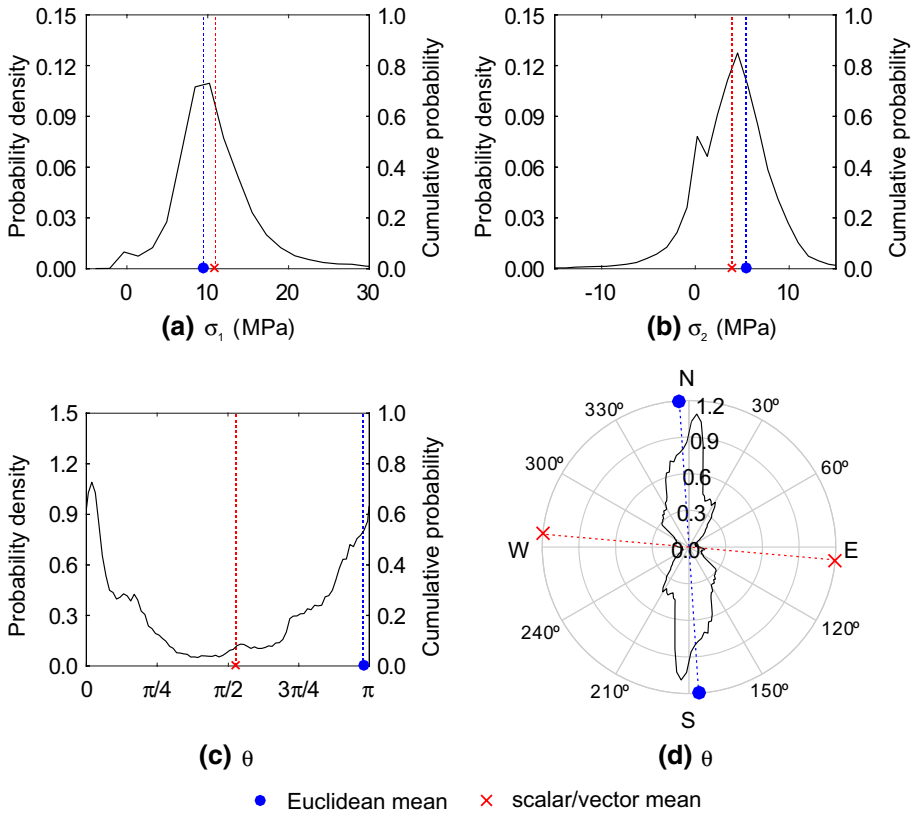


**Fig. 9** Probability density distributions of the principal stress magnitude ($\sigma_1$ and $\sigma_2$) and orientation ($\theta$) of the simulated stress data, and their scalar/vector and Euclidean means. Note that **c** and **d** show the probability density distribution of $\theta$ in rectangular and polar coordinate systems, respectively. For improved visualisation in **d**, the probability density distribution, which has a period of $\pi$, has been duplicated from the range $[0,\ \pi]$ to the range $[\pi,\ 2\pi]$. The dashed lines corresponding to the scalar/vector and Euclidean means are plotted to facilitate visualisation

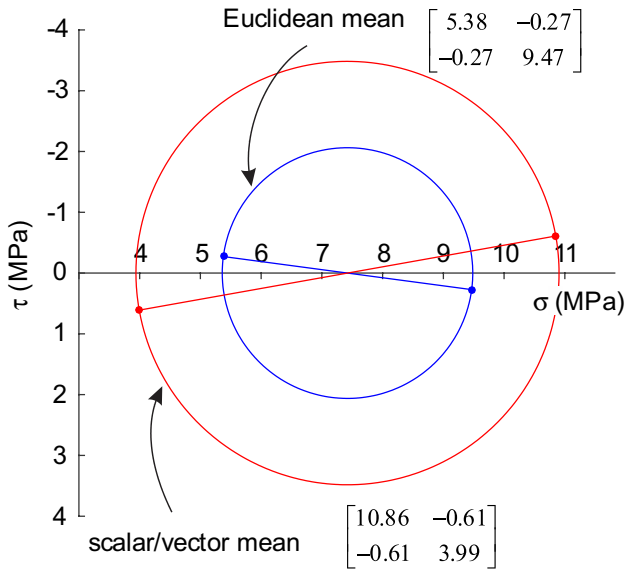


**Fig. 10** Mohr's circles of the Euclidean mean and scalar/vector mean

simulated stress data are calculated and shown in Table 6. It is worth noting that the correlation coefficients are calculated only for the purpose of illustrating the dependence between the principal stress magnitudes and orientations, and the non-zero correlation coefficients shown in Table 6 clearly reveal the dependence between $\sigma_1$ and $\sigma_2$ and $\theta$. Note

**Table 6** Correlation coefficients between the principal stress magnitude and the orientation $\theta$ of the two-dimensional simulated stress data

| Correlation coefficients | $\sigma_1$ | $\sigma_2$ | $\theta$ |
|---|---|---|---|
| $\sigma_1$ | 1.00 | 0.39 | 0.16 |
| $\sigma_2$ | | 1.00 | 0.18 |
| $\theta$ | *sym* | | 1.00 |

that for these data, the null hypotheses that the true correlation between any pairs of $\sigma_1$, $\sigma_2$ and $\theta$ is zero are rejected—in favour of the alternative hypotheses that they are not equal to zero—at the commonly used significance level of 5%. Therefore, the scalar/vector approach of processing principal stress magnitudes and orientations as independent quantities is erroneous. The tensorial approach, which averages the tensors that carry not only the information of stress magnitudes and orientations, but also the inherent connection between them, is thus more reasonable and appropriate.

We noted earlier that the scalar/vector mean tends to give larger mean $\sigma_1$ and smaller $\sigma_2$ than that does the Euclidean mean. Using the simulated stress data, we further investigate the possibility of the scalar/vector approach generating extreme mean principal magnitudes. The investigation is conducted by first randomly sampling a certain number of stress tensors (say, 2, 5, 10, 20, 50 and 100) from the 72,272 sampled simulated stresses and calculating both their scalar/vector and Euclidean mean. Then the sampling procedure

is repeated 10,000 times to obtain a series of mean stresses, and their probability density distributions are calculated. The results are presented in Fig. 11. From this, we observe that the scalar/vector mean of the major principal stress $\sigma_1$ is generally larger than that of the Euclidean mean, while for the mean minor principal stress $\sigma_2$, the opposite is true, i.e., the scalar/vector means are smaller than the Euclidean means. Additionally, as the sampling size increases, the probability density distributions of both the scalar/vector and Euclidean mean become more concentrated and the difference between them more distinct, which implies an increasing probability that the scalar/vector approach will generate extreme mean principal stress magnitudes that deviate more from the Euclidean mean. These random samplings suggest that when more in situ stress data are averaged (say, more than 10), there is a greater chance of the scalar/vector approach producing incorrect estimates of mean stress.

Although here for smaller sample sizes, the difference between Euclidean mean and scalar/vector mean are relatively small, it does not mean that the erroneous scalar/vector approach should be used in such circumstances. As can be seen from the case in Sect. 2 which averages only two stresses, a significant difference between the Euclidean mean and scalar/vector mean can also be found. Furthermore, and most significantly, there is no guarantee that the scalar/vector approach will produce orthogonal principal stresses. Thus, using the scalar/vector mean stress of in situ stress measurements as input to further rock engineering design or numerical simulations may have the potential to yield significantly erroneous results. Calculation of the tensorial Euclidean mean is straightforward, and as it is the correct approach, it is the one that should always be adopted.

## 5 Conclusions

We have examined the customary scalar/vector mean stress calculation approach that separately averages the principal stress magnitudes and orientations and compared it with the tensorial approach—Euclidean mean—that directly averages the stress tensors obtained in a common Cartesian coordinate system. We show how the scalar/vector mean may deviate from the Euclidean mean and test the appropriateness of both approaches.

Averaging two stress tensors reveals that the scalar/vector approach fails to interpret a simple physical case of superposition, and also gives non-unique mean values. On the other hand, the Euclidean mean is loyal to the tensorial nature of stress and gives physically reasonable and unique results. Application of the two methods to actual stress data demonstrates that the scalar/vector mean principal stresses may deviate significantly from that of the Euclidean mean, and the scalar/vector approach may yield non-orthogonal mean principal stresses, which is in contrast with the Euclidean mean that always generates orthogonal results.

Calculation of the means of randomly sampled simulated stresses obtained using FEMDEM shows that the scalar/vector mean generally yields larger major and smaller minor principal stress magnitudes than the Euclidean mean, and the scalar/vector mean principal stress orientation differs significantly from that associated to the Euclidean mean. As the sampling size increases, the probability of the scalar/vector approach generating extreme mean principal stress magnitudes increases.

Our calculations and comparisons lead us to conclude that the scalar/vector approach is deficient in that it processes the

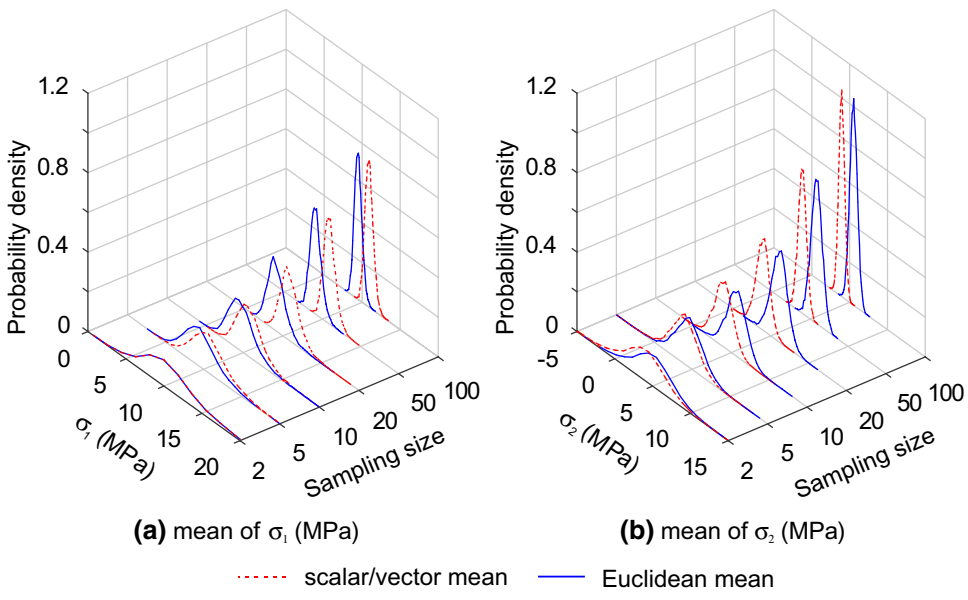


**Fig. 11** Probability density distributions of the mean principal stress magnitudes of the stress tensors sampled from the simulated stress data

principal stress magnitudes and orientations separately as independent quantities and ignores the connection between them. The tensorial approach averages the tensors and considers the contributions of and relation between stress magnitude and orientation, and is thus more reasonable and appropriate. Given the above-mentioned shortcomings, using the scalar/vector mean of in situ stress measurements as input in rock engineering design or numerical simulation may yield erroneous results. Calculation of the tensorial Euclidean mean is straightforward, and as it is the correct approach, it is the one that should always be adopted when processing stress data.

**Acknowledgements** We acknowledge the support of the NSERC (Canada) Discovery Grant (no. 491006) and the University of Toronto. The very valuable suggestions and comments of our colleague Dr. Nezam Bozorgzadeh are highly appreciated.

## References

Amadei B, Stephansson O (1997) Rock stress and its measurement. Springer, London

Belayneh MW, Matthai SK, Blunt MJ, Rogers SF (2009) Comparison of deterministic with stochastic fracture models in water-flooding numerical simulations. AAPG Bull 93(11):1633–1648

Brady BHG, Brown ET (2004) Rock mechanics for underground mining. Springer, The Netherlands

Brown ET, Hoek E (1978) Trends in relationships between measured in-situ stresses and depth. Int J Rock Mech Min Sci Geomech Abstr 15(4):211–215

Bulmer MG (1979) Principles of statistics. Dover Publications, New York

Chandler NA (2003) Twenty years of underground research at Canada's URL. In: WM'03 conference, Tucson, USA

Davis JC (1986) Statistics and data analysis in geology, 2nd edn. Wiley, New York

Day-Lewis AD (2008) Characterization and modeling of in situ stress heterogeneity. Ph.D. thesis, Stanford University, California, USA

Dyke CG, Hyett AJ, Hudson JA (1987) A preliminary assessment of correct reduction of field measurement data: scalars, vectors and tensors. In: Sakurai S (ed) Proceedings of 2nd international symposium on field measurements in geomechanics, Kobe, Japan. Balkema, pp 1085–1095

Dzik EJ, Walker JR, Martin CD (1989) A computer program (COSTUM) to calculate confidence intervals for in situ stress measurements, vol 1. Atomic Energy of Canada Ltd. Limited report AECL-9575, Canada

Gao K (2017) Contributions to tensor-based stress variability characterisation in rock mechanics. Ph.D. thesis, University of Toronto, Canada

Gao K, Harrison JP (2014) An aleatory model for in situ stress variability: application to two dimensional stress. In: Labuz JF (ed) 48th US rock mechanics/geomechanics symposium. American Rock Mechanics Association, Minneapolis

Gao K, Harrison JP (2015) Statistical calculation of mean stress tensor using both Euclidean and Riemannian approaches. In: Schubert W (ed) ISRM symposium EUROCK 2015 and 64th geomechanics collquy, Salzburg, Austria. Austrian Society for Geomechanics

Gao K, Harrison JP (2016a) Characterising stress dispersion for stress variability analysis. In: Johansson E (ed) RS2016 on symposium—7th international symposium on in-situ rock stress. International Society for Rock Mechanics, Tampere

Gao K, Harrison JP (2016b) Mean and dispersion of stress tensors using Euclidean and Riemannian approaches. Int J Rock Mech Min Sci 85:165–173. https://doi.org/10.1016/j.ijrmms.2016.03.019

Gao K, Harrison JP (2017) Generation of random stress tensors. Int J Rock Mech Min Sci 94:18–26. https://doi.org/10.1016/j.ijrmms.2016.12.011

Gao K, Harrison JP (2018a) Multivariate distribution model for stress variability characterisation. Int J Rock Mech Min Sci 102:144–154. https://doi.org/10.1016/j.ijrmms.2018.01.004

Gao K, Harrison JP (2018b) Scalar-valued measures of stress dispersion. Int J Rock Mech Min Sci 106:234–242. https://doi.org/10.1016/j.ijrmms.2018.04.008

Gao K, Lei Q (2018) Influence of boundary constraints on stress heterogeneity modelling. Comput Geotech 99:130–136. https://doi.org/10.1016/j.compgeo.2018.03.003

Gao K, Harrison JP, Lei Q, Latham J-P (2017) Investigating the relationship between far-field stress and local values of the stress tensor. Procedia Eng 191(Supplement C):536–542. https://doi.org/10.1016/j.proeng.2017.05.215

Hakala M, Ström J, Nujiten G, Uotinen L, Siren T, Suikkanen J, Oy P (2014) Thermally induced rock stress increment and rock reinforcement response, working report 2014-32. Posiva Oy, Helsinki, Finland

Hakami E (2011) Rock stress orientation measurements using induced thermal spalling in slim boreholes, R-11-12. SKB, Helsinki, Finland

Han J, Zhang H, Liang B, Rong H, Lan T, Liu Y, Ren T (2016) Influence of large syncline on in situ stress field: a case study of the Kaiping Coalfield, China. Rock Mech Rock Eng. https://doi.org/10.1007/s00603-016-1039-4

Harrison JP, Xiang J, Latham J-P (2010) Stress heterogeneity in a fractured rock mass modelled with the combined finite–discrete element method. In: 44th US rock mechanics symposium and 5th US–Canada rock mechanics symposium. American Rock Mechanics Association, Salt Lake City

Hast N (1969) The state of stress in the upper part of the earth's crust. Tectonophysics 8(3):169–211

Herget G (1988) Stresses in rock. Balkema, Rotterdam

Hudson JA, Cooling CM (1988) In Situ rock stresses and their measurement in the U.K.—Part I. The current state of knowledge. Int J Rock Mech Min Sci Geomech Abs 25(6):363–370

Hudson JA, Harrison JP (1997) Engineering rock mechanics—an introduction to the principles. Elsevier, Oxford

Hyett AJ (1990) Numerical and experimental modelling of the potential state of stress in a naturally fractured rock mass. Ph.D., University of London, London

Hyett AJ, Dyke CG, Hudson JA (1986) A critical examination of basic concepts associated with the existence and measurement of in situ stress. In: Stephansson O (ed) ISRM international symposium on rock stress and rock stress measurements. International Society for Rock Mechanics, Stockholm, pp 387–396

Jupe AJ (1994) Confidence intervals for in situ stress measurements. Int J Rock Mech Min Sci Geomech Abstr 31(6):743–747. https://doi.org/10.1016/0148-9062(94)90013-2

Koptev AI, Ershov AV, Malovichko EA (2013) The stress state of the Earth's lithosphere: results of statistical processing of the world stress-map data. Moscow Univ Geol Bull 68(1):17–25

Latham J-P, Xiang J, Belayneh M, Nick HM, Tsang C-F, Blunt MJ (2013) Modelling stress-dependent permeability in fractured rock including effects of propagating and bending fractures. Int J Rock Mech Min Sci 57:100–112

Lei Q, Gao K (2018) Correlation between fracture network properties and stress variability in geological media. Geophys Res Lett. https://doi.org/10.1002/2018GL077548

Lei Q, Latham J-P, Xiang J, Tsang C-F, Lang P, Guo L (2014) Effects of geomechanical changes on the validity of a discrete fracture network representation of a realistic two-dimensional fractured rock. Int J Rock Mech Min Sci 70:507–523

Lisle RJ (1989) The statistical analysis of orthogonal orientation data. J Geol 97(3):360–364

Mardia KV (1972) Statistics of directional data. Academic Press, London

Martin CD (1990) Characterizing in situ stress domains at the AECL underground research laboratory. Can Geotech J 27(5):631–646

Martin CD (2007) Quantifying in situ stress magnitudes and orientations for Forsmark: Forsmark stage 2.2, R-07-26. SKB, Sweden

Martin CD, Christiansson RC (1991a) Overcoring in highly stressed granite—the influence of microcracking. Int J Rock Mech Min Sci Geomech Abstr 28(1):53–70

Martin CD, Christiansson RC (1991b) Overcoring in highly stressed granite: comparison of USBM and modified CSIR devices. Rock Mech Rock Eng 24(4):207–235

Martin CD, Simmons GR (1993) The Atomic Energy of Canada Limited Underground Research Laboratory: an overview of geomechanics characterization. In: Hudson JA (ed) Comprehensive rock engineering, vol 3. Pergamon Press, Oxford, pp 915–950

Martin CD, Read RS, Lang PA (1990) Seven years of in situ stress measurements at the URL an overview. In: Hustrulid W, Johnson G (eds) 31th US symposium on rock mechanics. American Rock Mechanics Association, Golden

Martin CD, Kaiser PK, Christiansson RC (2003) Stress, instability and design of underground excavations. Int J Rock Mech Min Sci 40(7–8):1027–1047

Matsumoto S, Katao H, Iio Y (2015) Determining changes in the state of stress associated with an earthquake via combined focal mechanism and moment tensor analysis: application to the 2013 Awaji Island earthquake. Jpn Tectonophy 649:58–67

Munjiza AA (2004) The combined finite–discrete element method. Wiley, Hoboken

Munjiza A, Andrews KRF, White JK (1999) Combined single and smeared crack model in combined finite–discrete element analysis. Int J Numer Methods Eng 44(1):41–57

Obara Y, Sugawara K (2003) Updating the use of the CCBO cell in Japan: overcoring case studies. Int J Rock Mech Min Sci 40(7–8):1189–1203

Rougier E, Knight EE, Sussman AJ, Swift RP, Bradley CR, Munjiza A, Broome ST (2011) The Combined finite–discrete element method applied to the study of rock fracturing behavior in 3D. In: 45th U.S. rock mechanics/geomechanics symposium, San Francisco. American Rock Mechanics Association

Siren T, Hakala M, Valli J, Kantia P, Hudson JA, Johansson E (2015) In situ strength and failure mechanisms of migmatitic gneiss and pegmatitic granite at the nuclear waste disposal site in Olkiluoto, Western Finland. Int J Rock Mech Min Sci 79:135–148. https://doi.org/10.1016/j.ijrmms.2015.08.012

Valli J, Hakala M, Siren T (2016) Stress-geology interaction modelling at Olkiluoto. In: Johansson E (ed) RS2016 symposium—7th international symposium on in-situ rock stress. International Society for Rock Mechanics, Tampere

Veloso EE, Gomila R, Cembrano J, González R, Jensen E, Arancibia G (2015) Stress fields recorded on large-scale strike-slip fault systems: effects on the tectonic evolution of crustal slivers during oblique subduction. Tectonophysics 664:244–255

Walker JR, Martin CD, Dzik EJ (1990) Confidence intervals for In Situ stress measurements. Int J Rock Mech Min Sci Geomech Abstr 27(2):139–141

Xiang J, Munjiza A, Latham J-P (2009a) Finite strain, finite rotation quadratic tetrahedral element for the combined finite–discrete element method. Int J Numer Methods Eng 79(8):946–978

Xiang J, Munjiza A, Latham J-P, Guises R (2009b) On the validation of DEM and FEM/DEM models in 2D and 3D. Eng Comput 26(6):673–687

Zang A, Stephansson O (2010) Stress field of the Earth's crust. Springer, Berlin

Zhao XG, Wang J, Cai M, Ma LK, Zong ZH, Wang XY, Su R, Chen WM, Zhao HG, Chen QC, An QM, Qin XH, Ou MY, Zhao JS (2013) In-situ stress measurements and regional stress field assessment of the Beishan area. China Eng Geol 163:26–40

Zoback MD (2010) Reservoir geomechanics. Cambridge University Press, Cambridge